Efficient Global Sensitivity Analysis for Flow-Induced Vibration of a Nuclear Reactor Assembly using Kriging surrogates

Gregory A. Banyay[a,b], Michael D. Shields[c], and John C. Brigham[d,a]
[a]University of Pittsburgh, Department of Civil and Environmental Engineering, Pittsburgh, PA, USA
[b]Westinghouse Electric Company LLC, Cranberry Township, PA, USA [1]
[c]Johns Hopkins University, Department of Civil Engineering, Baltimore, MD, USA
[d]Durham University, Department of Engineering, Durham, UK

Abstract

In this work, surrogate modeling is used to support a global sensitivity analysis (GSA) for a nuclear reactor assembly as a proof-of-concept to demonstrate both the pertinence of such methods to this application as well as the significant physical insights provided by GSA. In addition to the knowledge gained relating to the system sensitivity, insight gained from the accuracy of the GSA results may be used to compare with goodness-of-fit metrics which are traditionally used to support the verification of the surrogate model. The coupled use of surrogate modeling and GSA reduces the number of full-order (i.e., standard computationally expensive finite element analysis) simulations required, substantially reducing total computational cost. This work focuses on the use of Kriging surrogates in particular, and examines the robustness of these techniques to evaluate sensitivity by considering a variety of design of experiment strategies used to create the surrogate models. Numerical experiments based upon an inverted top-hat upper internals assembly of a pressurized water reactor subjected to base motion and fluctuating lift and drag cross-flow loadings are used to evaluate the relationship between sensitivities computed from a full-order model versus those computed from a surrogate model, highlighting the effectiveness of utilizing GSA and surrogate modeling. For large sample sizes, negligible variation in the resultant sensitivities is shown with respect to the particular method by which a computational design of experiment is constructed to train the Kriging surrogates which lends credence to the stability and veracity of the results. Additionally, for the example presented herein the historical significance of the downcomer forcing function characterization is substantiated in the sense that loads from the downcomer which act indirectly on the upper internals are shown to dominate the response relative to direct-applied cross-flow loads.

Introduction

In accordance with guidance provided by the United States Nuclear Regulatory Commission (NRC) (United States Nuclear Regulatory Commission, 2017), new reactor designs are to complete a Comprehensive Vibration Assessment Program (CVAP) to evaluate Flow-Induced Vibration (FIV). License renewals similarly need to satisfy (United States Nuclear Regulatory Commission, 2017), but usually do so by demonstrating similarity to a valid prototype plant rather than completing a full analysis and test program, depending on the plant licensing basis. The CVAP includes extensive computational dynamic analysis, as described in (Westinghouse Electric Company, 2011), as well as a companion measurement and inspection program. The measurement and inspection program, as described in (Westinghouse Electric Company, 2015), recommends placing sensors in the locations which are dynamically correlated to the component response quantity of interest, which is generally near locations of high cyclic stress intensity. Correspondingly, the vibration analysis program establishes expected measurements (predictions) and associated acceptance criteria, which are based on the material fatigue life. Extensive verification and empirical validation of numerical models, for both forcing functions (e.g., turbulence and acoustic phenomena) and structural response, are employed to develop the predictions (Palamara, et al., 2015).

[1] Note that this paper reflects the views of the authors and not the views of Westinghouse Electric Company LLC.

Flow within a nuclear reactor coolant system is highly turbulent. The high turbulence is necessary for core cooling and heat transfer, but also creates a substantial vibratory forcing function on the associated mechanical components and assemblies. For analysis of reactor internals, M.K. Au-Yang developed methods for determining forcing functions in a downcomer annulus (Au-Yang & Jordan, 1980), modeling random vibration induced by turbulent flow (Au-Yang & Connelly, 1977), and summarized the majority of his published work in (Au-Yang, 2001). Guidelines for practice are then based on the work of Au-Yang and others for dynamic analysis of nuclear components subjected to flow-induced vibrations (ASME, 2017). Recent industry efforts such as (Banyay, et al., 2015) have sought to improve the methods described in (ASME, 2017) and part of the aim of this work is directed towards supporting such industry efforts to improve methods of dynamic analysis.

The forcing functions from turbulent flow acting on the various components of a nuclear reactor assembly can be characterized as a stochastic process (Tennekes & Lumley, 1972). As such, the dynamic structural response to turbulent loading is correspondingly random (Blevins, 2001). The spectral shape (i.e., the non-dimensional power spectral density, PSD) of the forcing random process may be known from prior test data of similar components in similar plants, but a best-estimate of the forcing function amplitude is generally difficult to determine. Note that within the nuclear industry, the term "best estimate" analysis has been defined as an analysis which is "free of deliberate pessimism regarding selected acceptance criteria" and "includes uncertainty analysis" (International Atomic Energy Agency, 2008). Therefore, in practice, plant designers use biased approaches which bound the scatter in the available data to characterize forcing functions. In so doing, this may produce conservative design margins, but can result in over-designed equipment and contribute to a lack of understanding of the actual structural dynamic behavior of critical components. Furthermore, such approaches can lead to misleading conclusions regarding the true design margin of a given component or system; contributing to a false sense of confidence in a high margin (Type II error) or a false impression that a component has a low margin (i.e., is at risk of failure, Type I error). Driven largely by recent major structural failures caused by FIV in the nuclear industry, such as the steam generators at San Onofre (United States Nuclear Regulatory Commission, 2015) or the steam dryer at Quad Cities (United States Nuclear Regulatory Commission, 2013), recent revisions to the NRC regulatory guide (United States Nuclear Regulatory Commission, 2017) increasingly demand that bias and uncertainty be accounted for in prototype reactor designs. Note that the industry guidelines offer some flexibility in the sense that they do not necessarily require rigorous uncertainty quantification but rather require that uncertainty and bias have been accounted for in the design process. For example, regulatory guidance accepts an extensive uncertainty analysis such as described in (ASME, 2009), but regulators also accept a more simple uncertainty analysis which demonstrates adequate bias to ensure conservative margins.

Within a reactor assembly, multiple forcing functions are present which are attributed to different excitation mechanisms that have to do with component geometry, local coolant velocities and temperature, spectral shape functions, and overall plant configuration (i.e., reactor coolant pump or piping design). These individual fluid-borne forcing functions, coupled with the structural dynamics, constitute the total observed structural response. From this total response, it is often unclear which particular forcing function is the most relevant for the response of a given component. The effect of the different forcing functions on the vibration response of a given component can vary significantly, with some having a relatively large effect and others being practically negligible. For example, the forcing function acting on an adjacent assembly (e.g., core barrel shell) may be more influential to the response of a given component (e.g., support columns or lower support structure) than the forcing function acting directly on that component. Misunderstanding the contributions of certain phenomenological behavior (e.g., the relative contribution of loads) can lead to excessive expense, such that analysts expend resources answering the wrong questions. For example, misunderstanding the contribution of boundary conditions and forcing functions to structural dynamic models may lead to studies employing

advanced Computational Fluid Dynamics (CFD) models to accurately characterize forcing functions that do not meaningfully influence the structural response. Variance-based sensitivity analysis can, in part, serve to reduce this excessive effort and cost (Saltelli, et al., 2008). For example, sensitivity analysis in this context could inform the selection of the parameters to which model outputs are most sensitive.

Variance-based global sensitivity analysis, such as described in (Saltelli, et al., 2008), (Gratiet, et al., 2016), (Cannavo, 2012), and (Pianosi, et al., 2015), requires running a model a large number of times to properly characterize the relative importance of the various uncertain parameters (Schenk & Schueller, 2005). It is therefore of interest to explore options to either reduce the number of full-order runs (i.e., finite element analysis realizations) required to characterize sensitivity, or to altogether replace the full-order model with a surrogate model which runs with minimal computational expense yet captures the relevant trends in the physical model. Surrogate modeling techniques aim to model physical phenomena using some means other than direct solution of the equations for the system physics. This is useful when solving the governing equations is computationally expensive or when the governing equations are not known and the trends must be inferred from data. Furthermore, several works have already applied the use of surrogate models for sensitivity analysis, successfully reducing the computational expense significantly such as (Shahsavani & Grimvall, 2011), (Hou, et al., 2016), (Cheng, et al., 2017).

Figure 1 shows an influence diagram used to construct an illustrative simplified cost-benefit analysis. In this postulated scenario, assumed cost quantities are shown in Table 1. These costs quantities are not arbitrary, but rather represent estimates based on approximately 10 years of performing such calculations in the industry. In the influence diagram, the "Analysis Method" parallelogram represents an index associated with three different approaches which may be taken to solve this problem. The "Number of Design Iterations" trapezoid is used to simulate how, as a design matures through time and thus iterates, the different analysis methods trend in terms of a cost comparison (which is represented by the hexagon). Design iterations are intended to represent a situation in which the physical geometry of a component changes, or a particular forcing function changes (perhaps due to an enhanced state of knowledge) and thus the dynamic response and corresponding ASME Code margins (i.e., design basis) change. In practice, both of these types of design iterations occur often, and this study considers the latter situation. That is, this study performs sensitivity studies on a fixed geometry and thus does not consider changes in geometric parameters, so the surrogates built and employed herein would not necessarily be valid in the context of geometry changes. Figure 2 then shows the results of how the engineering cost steadily increases when exercising a full-order model over many design iterations versus either supplementing a full-order model simulation with sensitivity analysis or by using a surrogate model in lieu of the full-order model (i.e., the items represented by the "Analysis Method" index). That is, significant savings may be realized by simply using the knowledge gained through sensitivity analysis to reduce complexity (i.e., the number of applied forcing functions) in the full-order model used for subsequent analyses in the design process; this is shown on the blue line in Figure 2. Further cost savings may be realized by altogether using a validated surrogate model in lieu of the full-order model in subsequent design iterations; this is shown on the green line in Figure 2. It is recognized that the veracity of a surrogate model requires that the parameter changes associated with the design iterations fall within the range of the parameter space sampled during initial model training. In practice therefore, there is a balance to achieve in which the sampled parameter space should be sufficiently large so as to bound the (future) parameter changes but not so large so as to render the initial problem computationally prohibitive. In short, if some initial investment is made upfront to understand parameter sensitivity for large dynamic models, then significant cost savings can be realized as the design iterates and subsequent simulations are required.

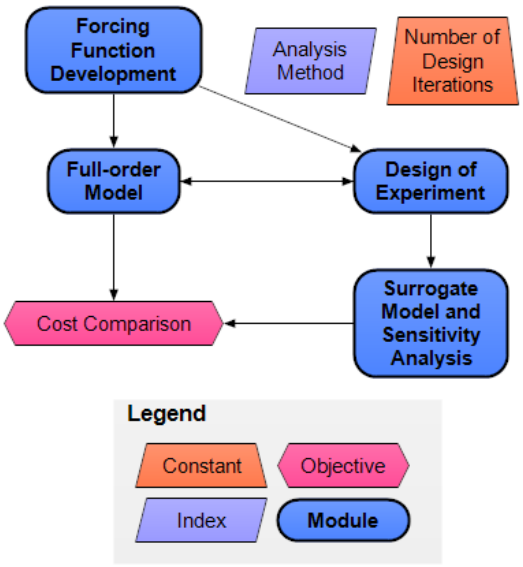

FIGURE 1 - INFLUENCE DIAGRAM AND INPUTS FOR POSTULATED COST-BENEFIT ANALYSIS

TABLE 1
COST-BENEFIT ANALYSIS VARIABLES

Variable	**Value**	**Comment**
Number of Design Iterations	10	Through the design and analysis of nuclear reactor structures, design parameters evolve, which warrants multiple iterations of computational models.
Cost of Full-order Model (per run)	10 hours	System finite element models subjected to dynamic FIV loading.
Cost of Initial Forcing Function Development (per function)	100 hours	Cost to run CFD and/or analyze test data to characterize forcing function. (e.g., boundary layer turbulence in downcomer annulus)
Number of Forcing Function Inputs	10	Multiple forcing functions acing on an assembly.
Number of runs needed for Design of Experiment	200	Number of full-order runs required for Surrogate model construction and/or Global Sensitivity Analysis (GSA).
Cost of Surrogate Model construction	10 hours	Time required to develop and train Surrogate model.
Cost of Surrogate Model run	0.1 hours	Representation of the small cost of Surrogate model runs (it is recognized that actual Surrogate model cost is well below 0.1 hours).

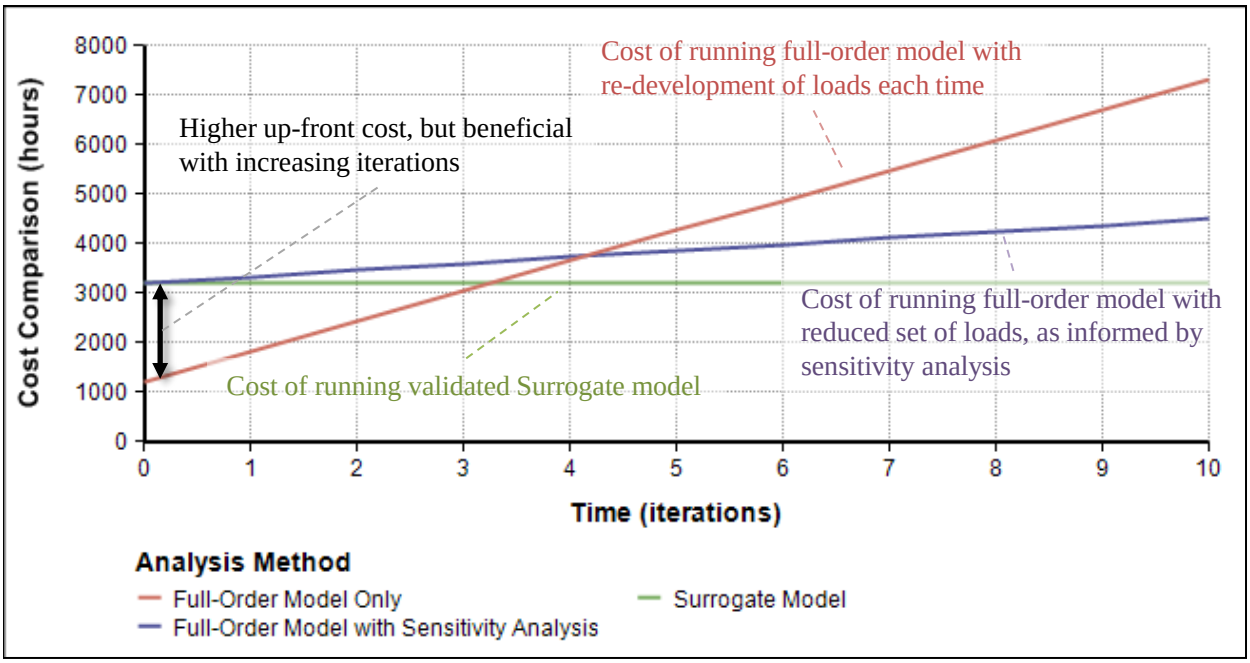

FIGURE 2 - ILLUSTRATION OF COST-BENEFIT ANALYSIS BETWEEN TRADITIONAL APPROACH AND THE USE OF SENSITIVITY ANALYSIS

In this work, a framework is developed to use surrogate models for sensitivity analysis for flow induced stationary random vibrations in a nuclear reactor internals subassembly, specifically to understand how forcing functions in different locations influence the response of the structure. This is intended to support fast turnaround analyses for experimental (real-time or near real-time) plant diagnostics, operational prognostics, and component design in the presence of parameter uncertainties. This research does not necessarily seek an optimal surrogate modeling technique, but rather a robust surrogate modeling technique that fits the specific application. For this purpose, Kriging (or Gaussian process regression) (e.g., (Nechak, et al., 2015) and (Huang, et al., 2011)) was used in this work. First, a full-order finite element model is used directly (i.e., without any complementary surrogate-model) to produce global sensitivity indices which do not meaningfully change upon generation of further full-order model realizations. By first computing sensitivity indices from full-order runs, this provides a set of results against which the surrogate-computed sensitivity indices may be compared. Given these "converged" sensitivity indices, the sampling of the parameter space for the full-order model runs is then investigated by considering a computational design of experiment using Latin Hypercube and Latinized Partially Stratified sampling techniques. Thus stability is evaluated in terms of the GSA result when the Kriging surrogate is trained by different sampling as a means of providing confidence in the surrogate-based sensitivities. One aim of this is to identify if it is practical to minimize the number of full-order runs required to re-generate sensitivity indices by way of a trained Surrogate model. It is expected that significant economic benefit may be realized in the engineering design process of nuclear reactor structures by coupling the advantages offered by both Surrogate modeling and GSA. The other aim, in this research, is to examine the relationship of the sensitivity indices to metrics in surrogate model validation. This is novel in the sense that observation of the error of the sensitivity indices relative to a baseline provides insight as to the veracity of the Surrogate model with which the sensitivity indices are computed.

The remainder of this paper is organized as follows. First, the methods utilized herein from each of the following three disciplines is described: Random Vibration, Surrogate Modeling, and Global Sensitivity Analysis. Then, a framework which combines these disciplines is described. A stationary random vibration

analysis which is typical of that used to simulate the dynamic response of a nuclear reactor assembly during plant operational conditions is described and exercised through this framework and the results are discussed, which is followed by the concluding remarks.

Methodology

In this study, the random vibration component corresponds to the finite element "full-order model" used to generate the baseline sensitivity indices, as well as to create the datasets to train the surrogate models – from which sensitivity indices will be likewise computed and verified against those from the full-order model. The overall methodology used seeks to combine the construction of a computational design of experiment (DOE), sensitivity analysis, and surrogate modeling as illustrated by the three parallel workflows in Figure 3. In the first workflow, GSA is performed on the full-order model using the Fourier Amplitude Sensitivity Test (FAST) algorithm as one means of computing sensitivity indices. This is done to establish the "true" sensitivity indices to compare with those computed by exercising a surrogate model. Using these full-order model evaluations from the FAST GSA, surrogate models for different numbers of realizations from the finite element analysis are constructed. In workflows 2 and 3, the full-order model is run using two different methods for computational DOE as an alternate means of building a surrogate model for GSA. The three workflows are then compared to evaluate the effectiveness of these different sampling methods for use in the FIV analysis of a nuclear reactor assembly as well as the stability of the GSA results computed from the various surrogates.

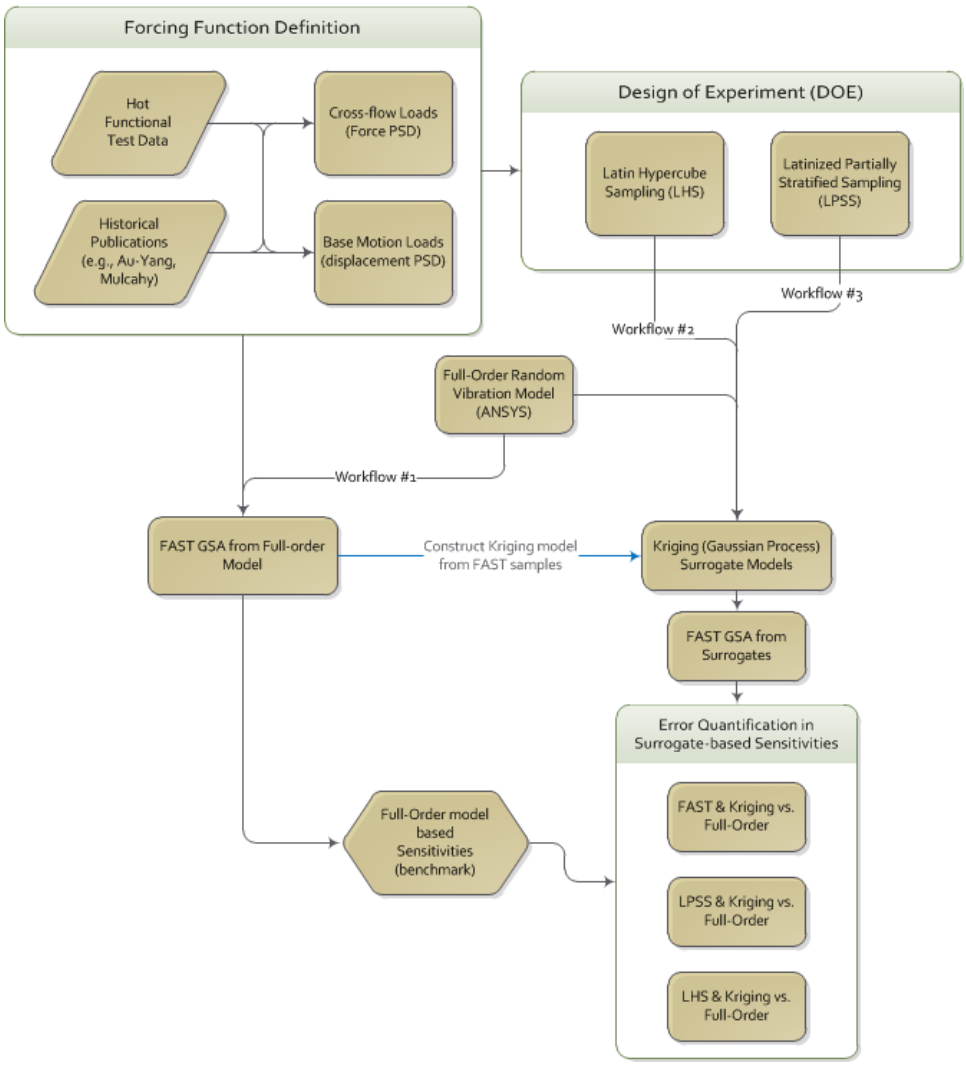

FIGURE 3 - FLOW CHART OF ANALYTICAL WORKFLOW INVOLVING MODEL DEFINITION, COMPUTATIONAL DOE, SURROGATE TRAINING, AND GSA

Random Vibration

Flow-induced random vibrations in reactor internals can often be characterized as stationary, ergodic random processes ((Tennekes & Lumley, 1972), (Blevins, 2001)). The stationary property follows from the steady-state operating conditions under which nuclear reactors typically operate; hence the vibration characteristics do not change with time. Thanks to the ergodic property, the mean and autocorrelation function of the forcing process, $z(t)$, can be defined, respectively, from a single realization as (Bendat & Piersol, 2010):

$$\mu = \lim_{T\to\infty} \frac{1}{T} \int_0^T z(t)\, dt \tag{1}$$

$$R_{zz}(\tau) = \lim_{T\to\infty} \frac{1}{T} \int_0^T z(t) z(t+\tau)\, dt \tag{2}$$

where τ is the time lag. The autocorrelation function may be thought of as a correlation between the values of the random process at two different times, t and $t + \tau$. Physically, τ should be chosen as a sufficiently small time lag as to resolve the highest frequencies of interest, which may pertain to the time scale of the dominant turbulent eddies or the dynamics of the structure itself.

The forcing random process (e.g., applied force and displacement loading) can be transformed to the frequency domain, with the autospectral density function given by the Wiener-Khintchine transform of the autocorrelation function:

$$G_{zz}(\omega) = \int_{-\infty}^{\infty} R_{zz}(\tau) e^{-\omega t}\ d\tau \tag{3}$$

The finite element method with modal superposition was used herein to solve for the system output PSDs (specifically, the commercial finite element analysis software ANSYS was used (ANSYS, 2016)). In particular, the natural frequencies, ω, and corresponding mode shapes, ϕ, of the structure were computed using the Lanczos algorithm (Rajakumar & Rogers, 1991). Then, the single degree-of-freedom (SDOF) transfer functions were used to calculate the response PSDs, as briefly outlined below.

Projecting the governing equations onto the system mode shapes, the equation of motion for modal dynamics of which a solution is sought may be expressed as:

$$\ddot{\delta}_j + 2\zeta_j \omega_j \dot{\delta}_j + \omega_j^2 \delta_j = F_j \tag{4}$$

where j is the mode number (from 1 to n), and δ, ω, and ζ, are the generalized displacement, frequency, and damping ratio for each of the modes, and F is the modal load. Then, using the modal analysis results, the forced vibration problem is solved in the frequency domain (Ortiz, et al., 1995).

Ultimately, this analysis is computing the mean squared axial strain response of the upper support skirt. Therefore, the following equations show the details necessary to obtain the RMS response from a PSD analysis.

Given the damping ζ at each mode j, the SDOF transfer function H for an input force may be computed as:

$$H_j(\omega) = \frac{1}{\omega_j^2 - \omega^2 + i\left(2\zeta_j \omega_j \omega\right)} \tag{5}$$

Next, the modal PSDs are then expressed in terms of these transfer functions and mode superposition as:

$$\begin{gathered} R_{jk}(\omega) = \sum_{l=1}^{r_1} \sum_{m=1}^{r_1} \gamma_{lj} \gamma_{mk} H_j^*(\omega) H_k(\omega) \bar{G}_{lm}(\omega) \\ \bar{R}_{lm}(\omega) = \frac{1}{\omega^4} \hat{G}_{lm}(\omega) \\ \hat{R}_{jl}(\omega) = -\frac{1}{\omega^2} \Gamma_{mj} H_j(\omega) \hat{G}_{lm}(\omega) \end{gathered} \tag{6}$$

where γ_{lj} and γ_{mk} are the participation factors from the modal analysis for modes j and k, respectively, corresponding to force excitation l and m, respectively, and H^* indicates the complex conjugate of H. $\bar{S}_{lm}(\omega)$ and $\hat{S}_{lm}(\omega)$ represent the input force and acceleration PSDs, respectively, which come from the forcing function development in this case. The number of mode shapes is denoted by n, and the number of nodal and base PSDs is denoted by r_1 and r_2, respectively. For the problem studied in this paper, all forcing functions are defined as force or acceleration PSDs acting on un-constrained nodes (i.e., not imposed at the support locations).

The strain terms may be expressed in terms of the modal PSDs, R, as dynamic, pseudo-static, and covariance parts, where $\bar{\phi}$ and $\bar{A}$ are the modal strains and static strains:

$$G_{d_i}(\omega) = \sum_{j=1}^{n}\sum_{k=1}^{n} \bar{\phi}_{ij}\bar{\phi}_{ik}R_{jk}(\omega)$$

$$G_{s_i}(\omega) = \sum_{l=1}^{r_2}\sum_{m=1}^{r_2} \bar{A}_{il}\bar{A}_{im}\bar{R}_{lm}(\omega) \tag{7}$$

$$G_{sd_i}(\omega) = \sum_{j=1}^{n}\sum_{l=1}^{r_2} \bar{\phi}_{ij}\bar{A}_{il}\hat{R}_{jl}(\omega)$$

Finally, the mean square strain response (ϵ^2) may be expressed as:

$$\epsilon_{f_i}^2 = \int_0^\infty G_{d_i}(\omega)d\omega + \int_0^\infty G_{s_i}(\omega)d\omega + 2\left|\int_0^\infty G_{sd_i}(\omega)d\omega\right|_{Re} \tag{8}$$

in which $\int_0^\infty G_{d_i}(\omega)d\omega$ is the variance of the i^{th} relative (dynamic) free strains, $\int_0^\infty G_{s_i}(\omega)d\omega$ is the variance of the i^{th} pseudo-static strains, and $\left|\int_0^\infty G_{sd_i}(\omega)d\omega\right|_{Re}$ is the real part of the covariance between the static and dynamic strains. A summary of the relevant theory of stochastic dynamics may be found in (Ortiz, et al., 1995).

Surrogate Modeling via Gaussian Process Regression

In recent years, reduced-order modeling techniques (e.g. (Grigoriu, 2010), (Grigoriu & Field, 2014)) and surrogate modeling methods (e.g., (Paez, et al., 1997)) have gained popularity for random vibration problems. One popular surrogate modeling method is kriging, otherwise known as Gaussian process modeling or Gaussian process regression, which has been shown to be effective for stochastic structural dynamics. For example, Abbiati et al. (Abbiati, et al., 2017) successfully used Kriging in conjunction with hybrid simulation to establish an active learning method in the context of structural reliability analysis for seismic applications. Kriging has the advantage of providing an error metric in the variance of the surrogate model, and has been successfully studied alongside methods of sensitivity analysis (Gratiet, et al., 2016).

A kriging model, $\mathcal{M}^K$, serving as a surrogate for the full-order model $\mathcal{M}$ (e.g., the random vibration finite element model), is expressed in accordance with (Rasmussen & Williams, 2005), (Sacks, et al., 1989), and (Lataniotis, et al., 2017), in which the bold-faced variable indicate a vector quantity:

$$\mathcal{M}^K(x) = \boldsymbol{\beta}^T \boldsymbol{f}(\boldsymbol{x}) + \sigma^2 \boldsymbol{Z}(\boldsymbol{x}, \xi) \tag{9}$$

in which $\boldsymbol{\beta}^T \boldsymbol{f}(\boldsymbol{x})$ is the mean value (or trend) constructed from regression coefficients $\boldsymbol{\beta}$ and basis functions $\boldsymbol{f}(\boldsymbol{x})$. As is typical, the basis functions were taken as multivariate polynomials of the form $f_\alpha(\boldsymbol{x}) = \prod_{i=1}^{M} x^{\alpha_i}$ where α is a vector of indices that yield polynomials in the M input variables up to degree P. For this work, ordinary Kriging was used in which the mean (trend) had a constant yet unknown value, which may be simply expressed as $\boldsymbol{\beta}^T \boldsymbol{f}(\boldsymbol{x}) = \beta_1 f_1(x) = \beta_1$.

The second term in Eq. (9), $\sigma^2 Z(\boldsymbol{x}, \xi)$ is a zero-mean stationary Gaussian random process with variance σ^2 and autocorrelation function $R(\boldsymbol{x_i}, \boldsymbol{x_j}; \boldsymbol{\theta})$. For our purposes, we assume $R(\boldsymbol{x_i}, \boldsymbol{x_j}; \boldsymbol{\theta})$ is an n-dimensional separable ellipsoidal correlation function expressed as:

$$R(x, x'; \theta) = R(h), \quad \text{where} \qquad h = \sqrt{\sum_{i=1}^{M} \left(\frac{x_i - {x_i}'}{\theta_i} \right)^2} \tag{10}$$

Parameter estimates, such as detailed in (Lataniotis, et al., 2017) or (Sundar & Shields, 2018), yield a kriging model with mean predictor:

$$\mu_{\mathcal{M}^K}(\boldsymbol{x}) = \boldsymbol{f}(\boldsymbol{x})\widehat{\boldsymbol{\beta}} + \boldsymbol{r}(\boldsymbol{x})^{\boldsymbol{T}} \boldsymbol{R}^{-\boldsymbol{1}} (\boldsymbol{M} - \boldsymbol{F}\widehat{\boldsymbol{\beta}}) \tag{11}$$

and predictor variance

$$\sigma^2_{\mathcal{M}^K}(\boldsymbol{x}) = \hat{\sigma}^2 \left(1 - \boldsymbol{r}(\boldsymbol{x}) \boldsymbol{R}^{-\boldsymbol{1}} \boldsymbol{r}(\boldsymbol{x}) + \boldsymbol{u}(\boldsymbol{x})^{\boldsymbol{T}} (\boldsymbol{F}^{\boldsymbol{T}} \boldsymbol{R}^{-\boldsymbol{1}} \boldsymbol{F})^{-\boldsymbol{1}} \boldsymbol{u}(\boldsymbol{x}) \right) \tag{12}$$

where

$$\boldsymbol{u}(\boldsymbol{x}) = \boldsymbol{F}^{\boldsymbol{T}} \boldsymbol{R}^{-\boldsymbol{1}} \boldsymbol{r}(\boldsymbol{x}) - \boldsymbol{f}(\boldsymbol{x}) \tag{13}$$

and $\boldsymbol{r}(\boldsymbol{x})$ is the vector of cross-correlations between the samples $\boldsymbol{x_i}$ and the prediction point $\boldsymbol{x}$.

Computational Design of Experiments

Gaussian Process Regression, as detailed in the prior subsection, relies upon a training data set. Such training data sets were generated by exercising a full-order finite element model for which computational design of experiments were constructed using Latin Hypercube Sampling (LHS) and a generalized Latin Hypercube sampling method called Latinized Partially Stratified Sampling (LPSS) (Shields & Zhang, 2016). In contrast to random Monte Carlo sampling, LHS aims to spread the sample points evenly across all possible values. LHS partitions each input parameter distribution into intervals of equal probability, and selects one sample from each interval, and shuffles the sample for each input so that there is no correlation. The LPSS method performs simultaneous Latin sampling of all variables and stratified sampling of subsets of variables, and has been shown to provide variance reduction in the context of parameter interactions.

Global Sensitivity Analysis

While many methods of sensitivity analysis exist (Morgan, et al., 1992), global sensitivity analysis (GSA) is employed herein as a variance-based technique, which surveys the full parameter space. For this application, GSA provides insight as to the relative importance of multiple parameters (forcing functions), which mutually influence the forced response of interest. Furthermore, GSA accounts for uncertainty in the input parameter space so that each plausible combination of relative forcing function variations is considered.

First-order sensitivity indices for output $\epsilon = f(\boldsymbol{P})$ given input parameters $\boldsymbol{P} = (p_1, p_2, \dots, p_n)$ are defined as (Saltelli, et al., 2008):

$$S_i = \frac{V[E(\epsilon|p_i)]}{V(\epsilon)} \tag{14}$$

where V[·] denotes the variance operator. The expected value of $\boldsymbol{\epsilon}$ can be evaluated by the n dimensional integral:

$$E(\boldsymbol{\epsilon}) = \int_{I^n} f(p)dp \tag{15}$$

in which I^n is the n dimensional unit hypercube. The Fourier amplitude (FAST) method, is used for the present study to convert the n dimensional integral into a one-dimensional integral as a function of a new variable s as follows.

The essence of FAST is to generate a curve in the parameter space that is a periodic function of each parameter, with a different frequency for each. The contribution of each input is measured by the contribution of its characteristic frequency Ω_i to the outputs (Morgan, et al., 1992).

First, per (Cannavo, 2012) the function $f(\boldsymbol{P})$ may be expanded as:

$$f(\boldsymbol{P}) = f_0 + \sum_{s=1}^{n} \sum_{i_1<\cdots<i_s} f_{i_1 \dots i_s}(p_{i_1}, \dots, p_{i_s}) \tag{16}$$

This summation is over all possible combinations of s different input variables. The component $f(\boldsymbol{P}) = f_{i_1 \dots i_s}(p_{i_1}, \dots, p_{i_s})$ can then be expressed as a Fourier series:

$$f(\boldsymbol{P}) = \sum_{k_1=-\infty}^{\infty} \sum_{k_2=-\infty}^{\infty} \dots \sum_{k_n=-\infty}^{\infty} C_{k_1 k_2 \dots k_n} e^{j2\pi(k_1 p_1 + k_2 p_2 + \cdots + k_n p_n)} \tag{17}$$

With Fourier coefficients:

$$C_{k_1 k_2 \ldots k_n} = \int_{I^n} f(\boldsymbol{P}) e^{j2\pi(k_1 p_1 + k_2 p_2 + \cdots + k_n p_n)} d\boldsymbol{P} \tag{18}$$

The variances result in the sums of the parts of the Fourier coefficients:

$$V\{f_{i_1 \ldots i_s}\} = \sum_{k_{i_1}=-\infty}^{\infty} \ldots \sum_{k_{i_s}=-\infty}^{\infty} \left| C_{k_{i_1} \ldots k_{i_s}} \right| \tag{19}$$

In order to solve the n dimensional integral, every input is expressed as a function of a new independent variable s as:

$$p_i(s) = \frac{1}{2} + \sin^{-1}(\sin(\Omega_i s)) \tag{20}$$

Correspondingly, the expected value of y can then be expressed as $\frac{1}{2\pi}\int_{-\pi}^{\pi} f(s)ds$. Solution of this integral involves an analysis of variance (ANOVA) decomposition which includes the calculation of Fourier coefficients C_{k_i}, where index i pertains to the summation of the ANOVA. This method involves numerical integration of:

$$C_{k_i} = \frac{1}{2\pi} \int_{-\pi}^{\pi} f(s) e^{-j2\pi k_i \Omega_i s} ds \tag{21}$$

The number of discrete intervals used to evaluate this integral is defined by variable M. Per (McRae, et al., 1980), the choice of M and the number of inputs k govern the number of model runs used to compute the GSA indices. Since the number of inputs is set for the upper internals FIV study evaluated herein, the parameter M was adjusted to change the number of model runs used by the GSA. Finally, the numerator needed for computing the global sensitivity indices is calculated as:

$$E(y|p_i) = \sum_i \left| C_{k_i} \right| \tag{22}$$

Therefore, substituting Equation (22) into Equation (14) provides first-order global sensitivity indices:

$$S_i = \frac{V\left[\sum_i \left| C_{k_i} \right|\right]}{V(y)} \tag{23}$$

GSA for Upper Internals Model

First, the response of the upper internals assembly of a nuclear reactor subject to FIV is investigated. Per ASME Code design guidelines, as shown in Subsection NG of (ASME, 2017), and also for purposes of manufacturability and regulatory acceptance, reactor internal assembly core supports are generally constructed of geometrically simple shapes. As such, various structures, such as lower and upper support columns, can be rightly approximated as axisymmetric beams. As an example, Figure 4 shows an upper internals assembly for the AP1000 plant.

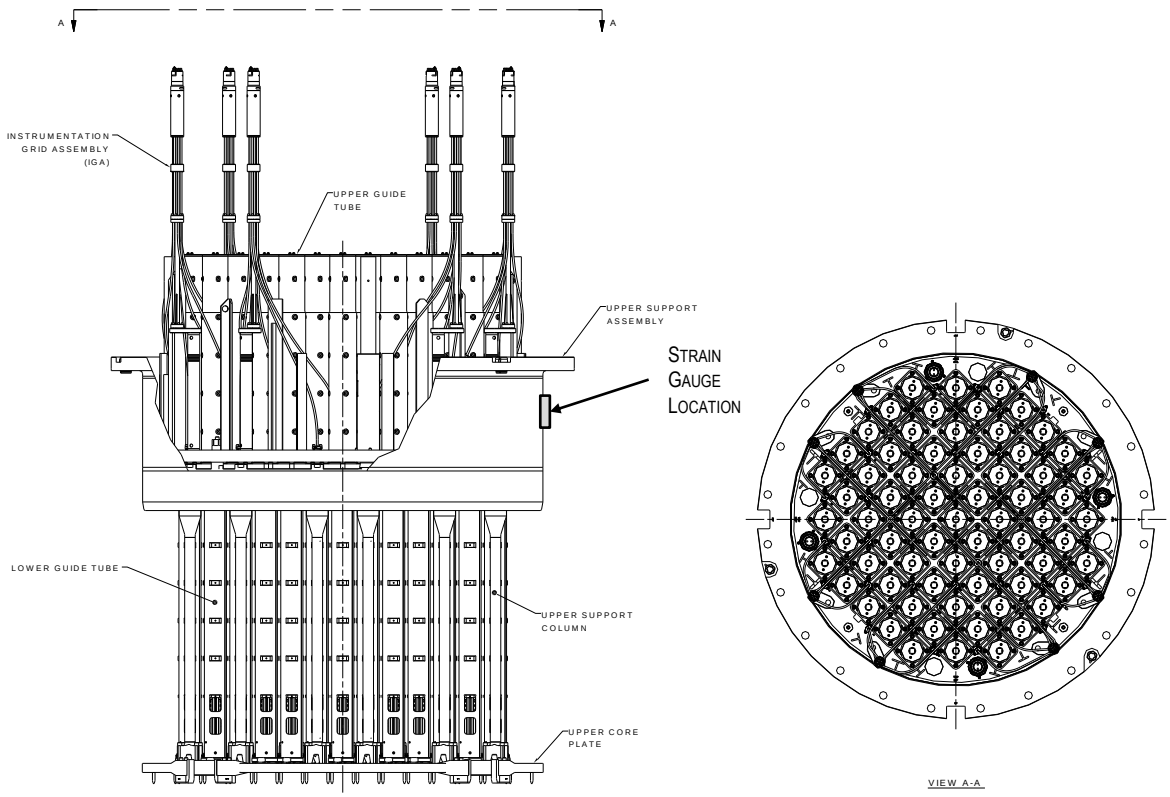

FIGURE 4 - UPPER INTERNALS ASSEMBLY FOR THE AP1000 PLANT (FROM (WESTINGHOUSE ELECTRIC COMPANY, 2011))

A simplified finite element model to solve the problem described above in the above Random Vibration Section of the assembly was built in ANSYS using linear hexahedral elements. The material was austenitic stainless steel with density 7,850 $\frac{kg}{m^3}$, Poisson's ratio 0.3, and elastic modulus $2 \times 10^{11} Pa$. The material was considered linear elastic and geometric nonlinearities were not considered. The structure was supported with simple supports at the top rim of the upper support skirt, in the sense that displacement was zero in all three translational degrees of freedom, and subjected to three direct-applied forcing functions to the support columns acting in the radially outward direction, lateral forcing functions on each of the upper core plate and upper support plate acting in mutually perpendicular directions, and a vertical forcing function on the upper core plate. The model, including boundary conditions and loads is shown in Figure 5. The output of interest from this model was assumed to be the axial (normal) strain, denoted ϵ, of the upper support skirt in the interest of simulating a virtual strain gauge measurement; see Figure 5. As a simplification for this study, fluid elements were not included. Although the surrounding fluid would impart an effective added mass to the structure, the

focus of this work lies in the application of GSA methods, and so the conclusions would not be impacted by this added mass effect.

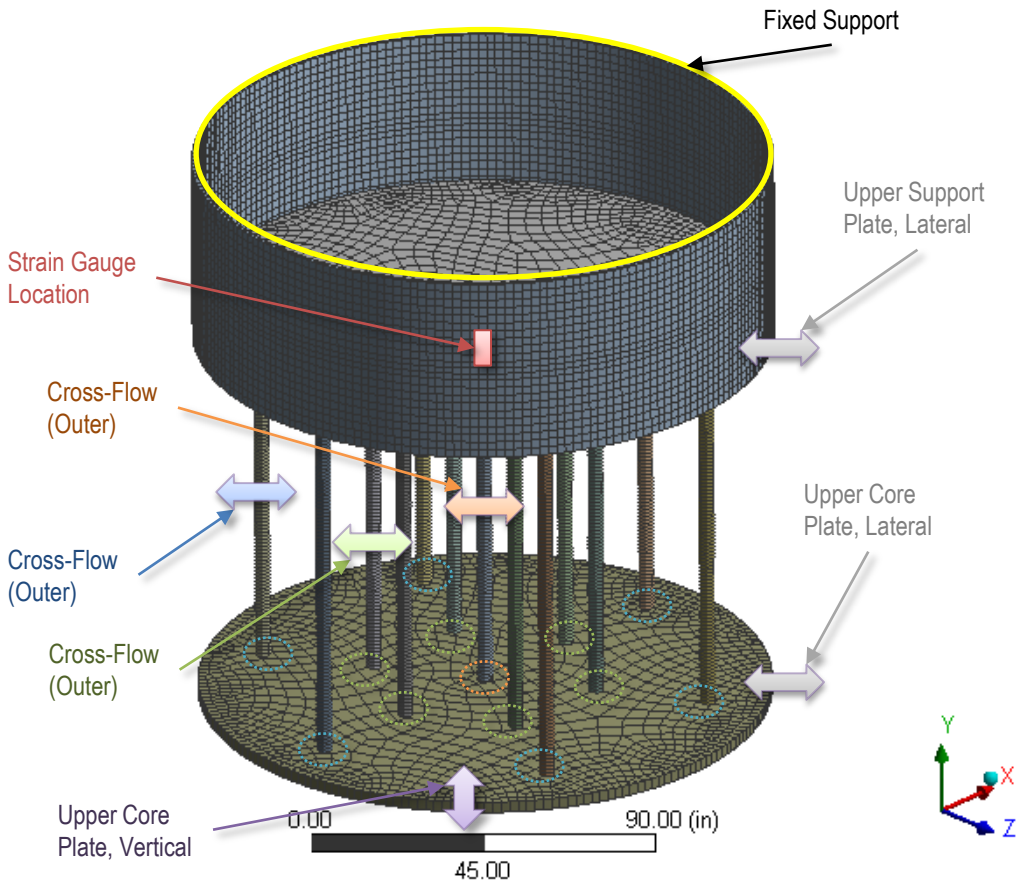

FIGURE 5 - UPPER INTERNALS MODEL, MESH, AND BOUNDARY CONDITIONS

Two types of loads were applied to the structure: 1. Cross-flow loads on the support columns, and 2. Base motions applied to the upper core plate and upper support plate. Cross-flow loads correspond to forces induced on the columns by turbulent flow of coolant over the columns. Here, cross-flow loads were modeled as a stochastic process that is fully correlated along the length of the column. To more accurately predict forced response, the cross-flow loading could be defined with an uncertain correlation length and permitted to vary between one and three diameters along the length of the column (consistent with that observed by Mulcahy for turbulent cross-flow (Mulcahy, 1982)). However, this was considered a secondary effect and, for this study, was not considered. The term "base motion" is used for displacements applied to the upper core plate and upper support plate as those loads are caused by adjacent reactor components which were not included in the finite element model (e.g., base motion imparted from the core barrel to the upper support plate).

Both the direct-applied and base motion loading were applied from 0 – 2,000 Hz with exponential spectral decay of $G(\omega) \propto \omega^{-1.75}$, as illustrated in Figure 6. This spectral decay appears consistent with the non-dimensional forced response PSDs provided by (Au-Yang & Jordan, 1980) and (Mulcahy, 1982). For comparison, forced response data from a column-like structure exposed to cross-flow loading from a CVAP

hot functional test program is shown in Figure 6 with dashed lines. The peaks in the forced response correspond to the natural frequencies of the structure, but it may be seen that the broadband decay of the applied forcing function is consistent with the data. Statistical analysis of this same dataset reveals that the forced response is Gaussian, ergodic and stationary.

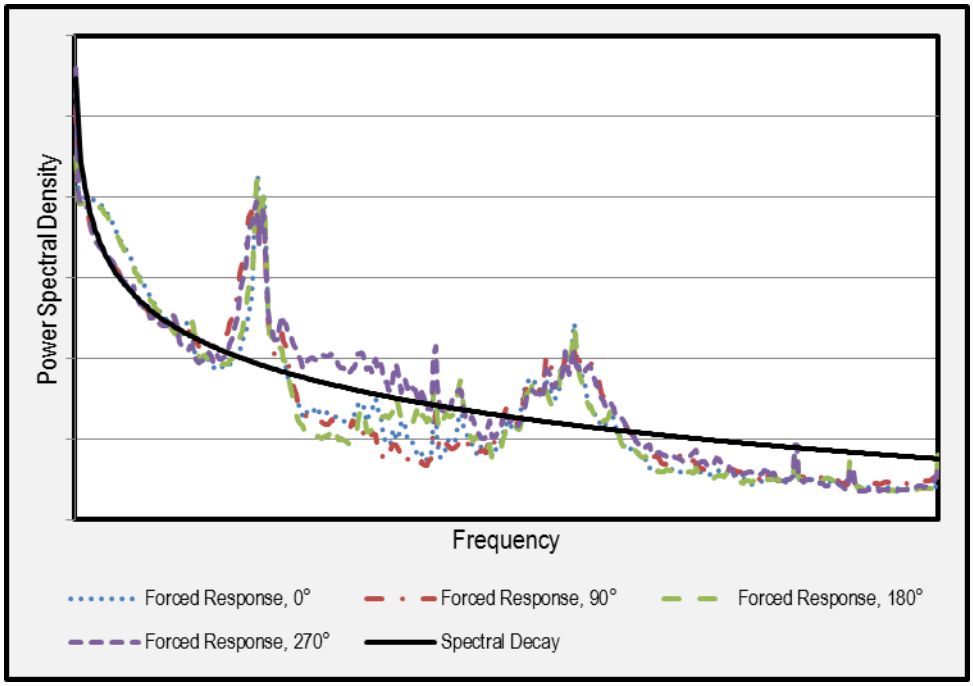

FIGURE 6 - FORCING FUNCTION NON-DIMENSIONAL POWER SPECTRAL DENSITY (WITH BEAM FORCED RESPONSE DATA OVERLAID)

For GSA, the magnitude of the PSD was scaled as shown by the λ terms in Table 2. In this analysis, the λ terms were assigned a Uniform distribution on the range $[0.9, 1.1]$, from which random samples were drawn for the computational DOE. A Uniform distribution was chosen because the expected value of the PSD for any of these forcing functions is of equivalent likelihood of falling anywhere within a ±10% about the nominal value. The magnitude of the force and displacement PSDs were chosen based on the approximate order of magnitude of which these loads have been recorded from various historical instrumented Hot Functional Tests and sub-scale tests of PWRs.

TABLE 2
FORCING FUNCTIONS APPLIED TO UPPER INTERNALS FINITE ELEMENT MODEL

Forcing Function	Type of Excitation	PSD Scaling
Cross-Flow across Support Columns	Force	$\tilde{G}_x^F(\omega)_{USC.Center} = \lambda_{USC.Center} \times G_x^F(\omega)$ $\tilde{G}_x^F(\omega)_{USC.Mid} = \lambda_{USC.Mid} \times G_x^F(\omega)$ $\tilde{G}_x^F(\omega)_{USC.Outer} = \lambda_{USC.Outer} \times G_x^F(\omega)$
Base motion applied to Upper Core Plate and Upper Support Plate	Displacement	$\tilde{G}_x^\delta(\omega)_{UCP.Edge} = \lambda_{UCP.Edge} \times G_x^\delta(\omega)$ $\tilde{G}_z^\delta(\omega)_{USP.Edge} = \lambda_{USP.Edge} \times G_z^\delta(\omega)$ $\tilde{G}_y^\delta(\omega)_{UCP.Face} = \lambda_{UCP.Face} \times G_y^\delta(\omega)$

Surrogate Model Verification

It is of interest to determine how the relative difference in sensitivity indices compares with an independent measure of surrogate model accuracy, such as the error between output strains predicted by the Surrogate model and an independent (i.e., not used to train the surrogate models) set of data from the full-order model. To examine this, 100 full-order simulations were sampled independent of the training sets of data used to establish the Surrogate models. Then, the trained Surrogate models were exercised on this independent dataset of 100 to evaluate how well the surrogate model estimations agreed with the full-order model results. The measure of error chosen for these tests was the Root Mean Square (RMS) error based on the Frobenius Norm, which may be defined as:

$$\|E\|_F \equiv \sqrt{\frac{1}{m}\sum_{i=1}^{m}\left|\left(\epsilon_{FullOrderModel} - \epsilon_{SurrogateModel}\right)_i\right|^2}$$

Where $\epsilon_{FullOrderModel} - \epsilon_{SurrogateModel}$ is the difference between the i^{th} result predicted by the Kriging model and the associated result of the full-order model. Variable ϵ represents the axial strain on the upper support skirt. Figure 7 shows the RMS error between the full-order model and surrogate models constructed from three different DOE strategies, LHS, LPSS, and FAST sample points, and each with a varying number of training datasets from 27 to 1,728. A steep decrease in error by approximately a factor of 10 is observed with increasing sample size beyond 64 for all Surrogates and, while some small variability is observed from the Surrogates which were trained from the different DOE methods, the error is less than 0.01 $\mu\epsilon$, and thus judged negligibly small, in every case for samples sizes of 125 and greater. The minimum number of samples studied for FAST was 393 based on the use of six random variables, per the (Cukier, et al., 1978) algorithm encoded in the SAFE toolbox (Pianosi, et al., 2015). Note that on this and subsequent similar figures, dotted or dashed lines in lieu of solid lines are used to indicate that data between the markers were not directly calculated in this work. For further comparison, these results were also compared with a Box-Behnken design (Montgomery, 2013) in the interest of understanding how such a traditional DOE approach may perform, and the RMS error of the Box-Behnken design was 15% higher than that associated with LHS, LPSS, and FAST.

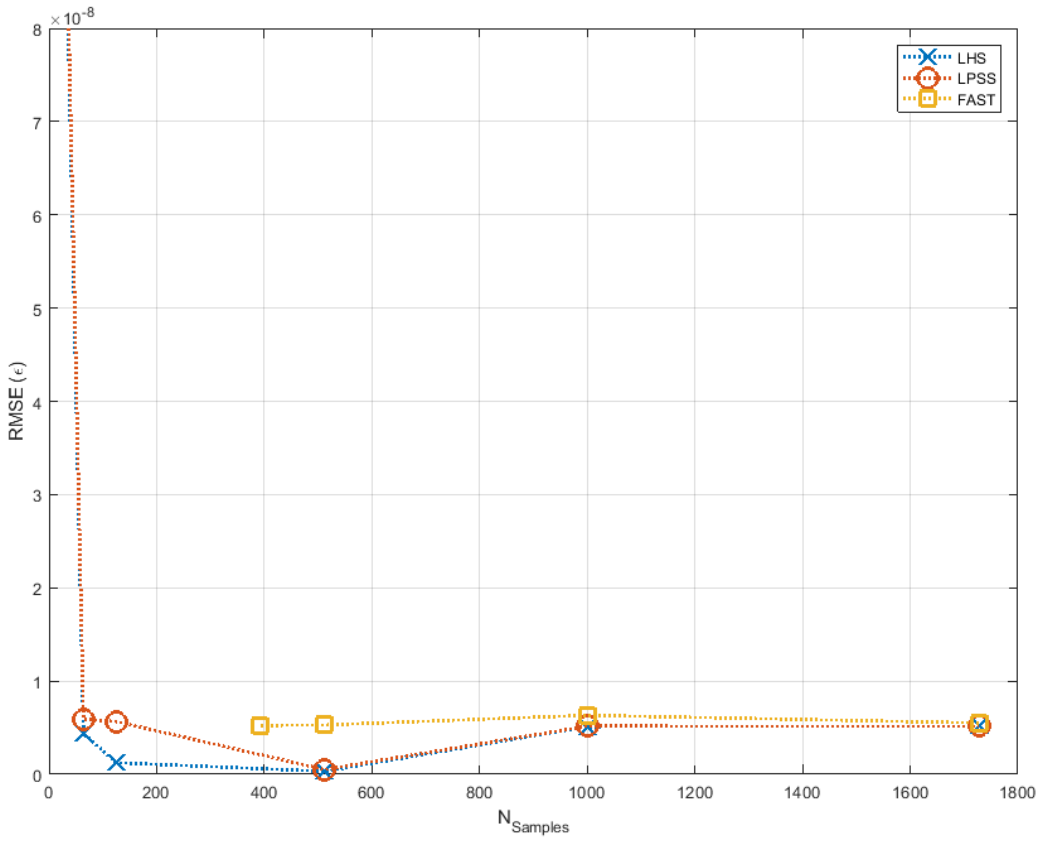

FIGURE 7 - SURROGATE MODEL VERIFICATION BY COMPARISON TO TEST SET USING ROOT MEAN SQUARED ERROR (MICROSTRAIN)

Global Sensitivity Analysis Results

Given some understanding of the accuracy of the Surrogate model, it is now of interest to examine the change in GSA results having to do with increasing the sample size and changing the sampling method. To that end, the following subsections present the results of the three workflows illustrated in Figure 3.

Prior to examining the results from each workflow, the physical significance of the GSA results is noteworthy. The GSA results from all workflows show that the base motion loads acting in the lateral direction at both the Upper Core Plate (UCP) and Upper Support Plate (USP) each account for 41% of the output variance, the UCP vertical forcing function accounts for 16% of the output variance, and the sum total of the direct-applied cross-flow loads account for less than 1% of the output variance. This is meaningful in the sense that the dynamic response of the upper internals assembly is governed more by turbulence which imparts loads to the interface joints (i.e., upper support flange) more so that turbulence which acts directly upon the upper support columns.

This sort of observation serves to inform key engineering decisions related to up-front design investments as well as in diagnostics during plant operation. For example, to borrow a principle of decision theory, the expected value of perfect information would be much greater to define the forces associated with base motion loads than direct-applied cross-flow loads, during the design stage of a new reactor. Correspondingly, given the extreme difficulty of placing sensors within an operating reactor environment, it is valuable to understand that measuring the flow field directly by placing a sensor within the upper plenum would provide very limited insight into the structural dynamic behavior of the upper internals structures.

Workflow 1: Full-Order Model GSA using FAST

Using the SAFE toolbox documented in (Pianosi, et al., 2015) (for which the underlying methodology is similar to that implemented in UQLab (Marelli & Sudret, 2014)), GSA was performed, first using the full-order model described. An increasing number of samples were generated for the 6 inputs to the full-order model until convergence of the sensitivity indices was observed. The number of simulations required to produce sensitivity indices that did not change more than 0.3% (or a sensitivity index magnitude of 0.0005) upon further samples was 5,000. Convergence of the sensitivity indices is plotted in Figure 8, from which it may be seen that there was no substantial change in the magnitude of the sensitivity indices as sample sizes greater than 512. Specifically, between 1,728 and 5,000 samples, the sensitivity indices associated with the base motion loads differed by less than 0.0005 and those associated with cross-flow loads differed by less than 3.6×10^{-5}.

Using the model evaluations from the FAST GSA, a kriging surrogate was built for four sample sizes. In so doing, this leverages the computational data already-accumulated from establishing the full-order model based sensitivity indices, without the need to generate additional model realizations from a computational DOE with some alternative sampling method such as LHS or LPSS. Then, in order to provide confidence in the robustness of using a surrogate for GSA, sensitivity indices from these surrogate models were calculated using FAST (implemented in SAFE (Pianosi, et al., 2015)), which are shown in Figure 9. The black circles on Figure 9 represent the benchmark sensitivities against which the surrogate-based sensitivities are compared (i.e., the sensitivities associated with 5,000 samples from Figure 8), and the differences between the surrogate-computed first order sensitivity indices S_1^{Surr} and those computed from the full-order model S_1^{FEA} are then shown on Figure 10. Given that this problem had 6 random inputs, the minimum number of samples evaluated using FAST was 393 (Cukier, et al., 1978), and the subsequent three sample sizes considered were 512, 1,000, and 1,728.

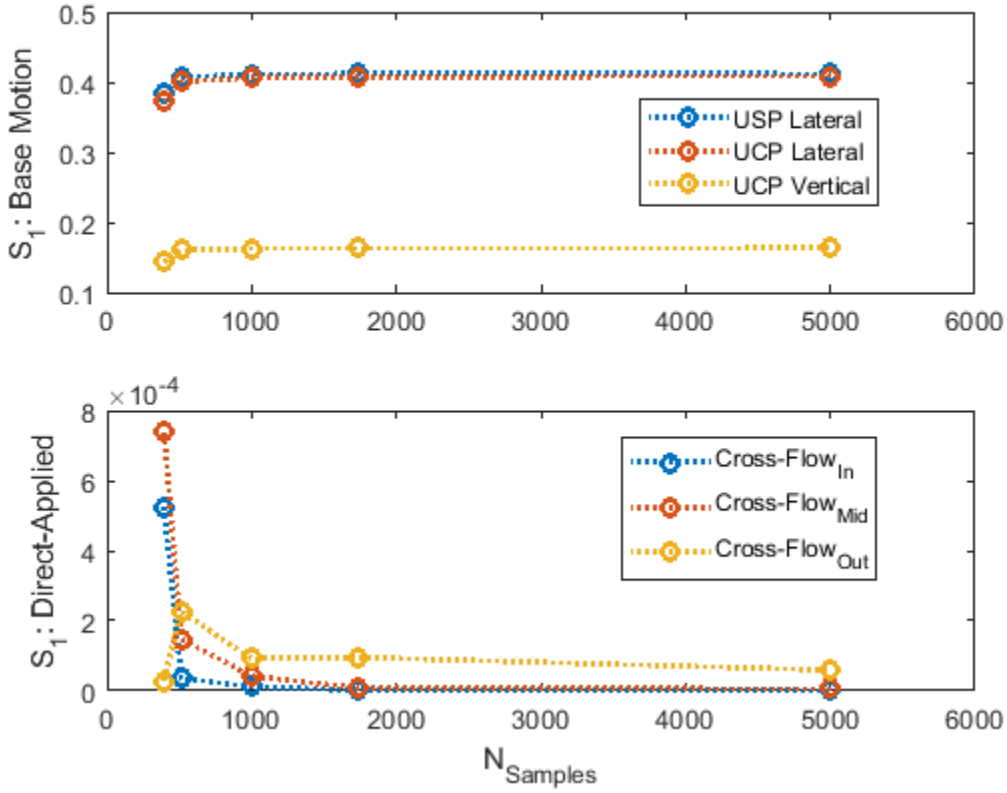

FIGURE 8 – FULL-ORDER MODEL GLOBAL SENSITIVITY ANALYSIS CONVERGENCE

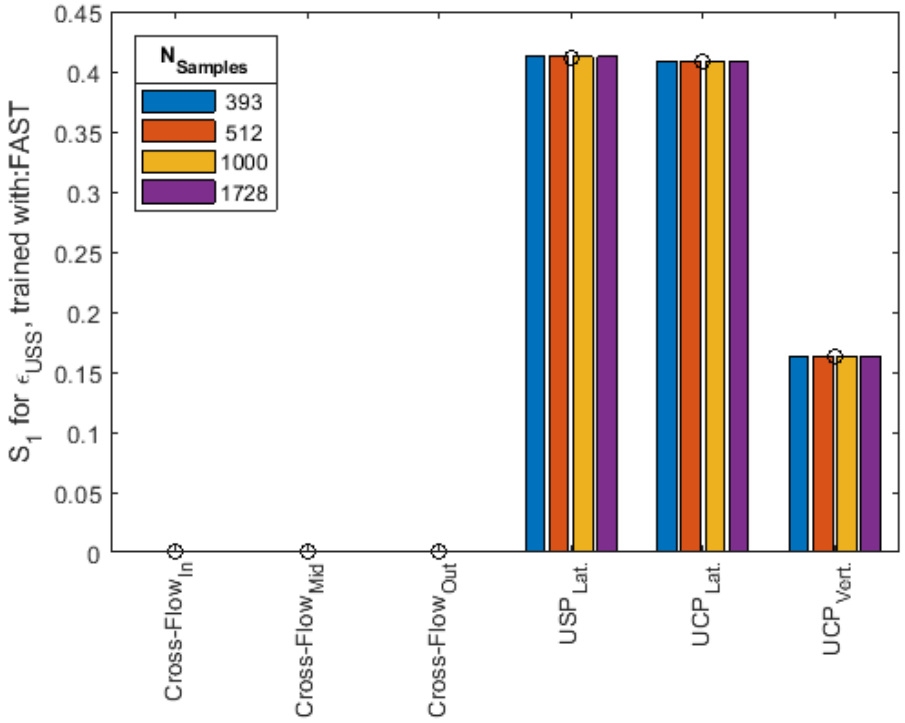

FIGURE 9 - GSA FROM KRIGING SURROGATES TRAINED WITH FAST AT VARYING SAMPLE SIZES

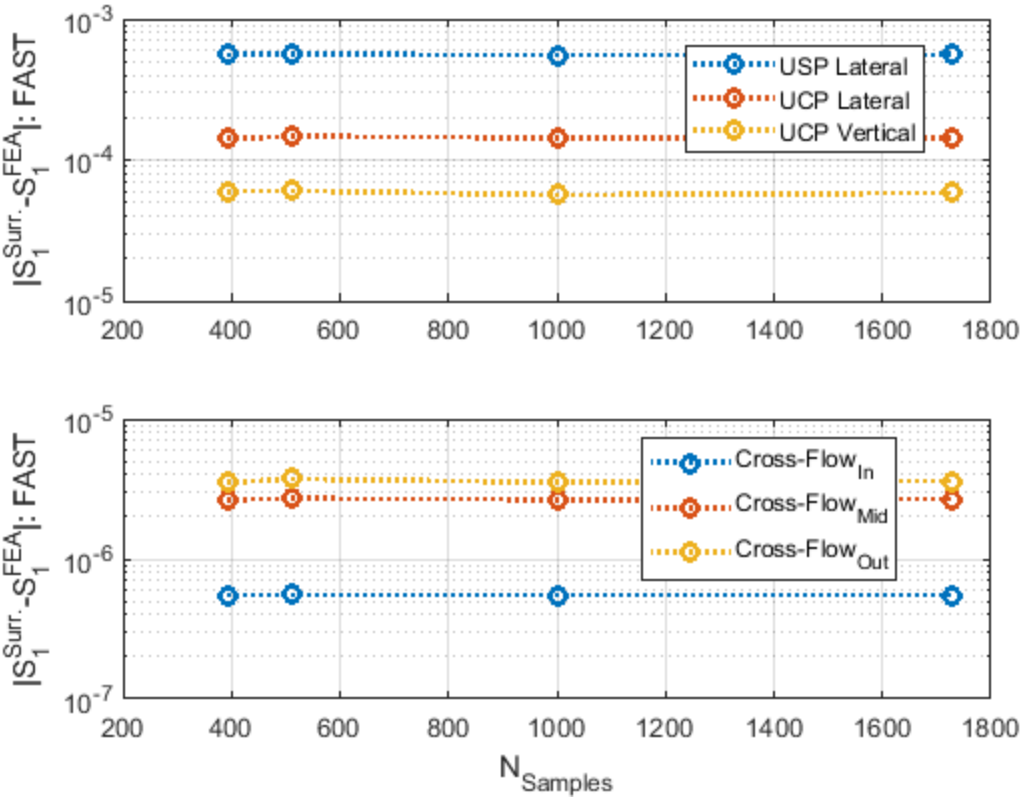

FIGURE 10 – FAST-TRAINED SURROGATE-BASED SENSITIVITIES VS BENCHMARK

Workflows 2-3: GSA from DOE-based surrogates

In workflows 2-3 from Figure 3, two different sampling methods of computational design of experiments were used to construct a surrogate model for GSA. Following Workflow 2, the kriging surrogate is constructed from samples generated by LHS. Following Workflow 3, the kriging surrogate is built from samples generated from LPSS. In this case we consider LPSS designs in which the crossflow loads are grouped for stratification and the base motion displacement loads are grouped for stratification. This LPSS design is described in Table 3 and results in samples sizes of 27, 64, 125, 512, 1000 and 1728 samples from which the surrogate model is trained. LHS of the same size are used for a fair comparison.

TABLE 3 - SETUP OF PARTIALLY STRATIFIED SAMPLING DESIGN

forcing function	**sub-domain dimension (N_i)**	**strata**	**number of samples**
cross-flow (inner, middle, outer on upper support column)	3	3 4 5 8 10 12	27 64 125 512 1000 1728
base motion (upper core plate, upper support plate, vertical)	3		
number of dimensions	6		

Global sensitivity analyses were then performed on the surrogate models in Workflows 2 and 3, again using FAST as implemented within (Pianosi, et al., 2015). For each sample size, the resultant first-order Sensitivity indices are shown in Figure 11 and Figure 12 based on LHS and LPSS, respectively, in which the black circles are the benchmark sensitivities computed from the full-order model directly. It may be seen that the sensitivities are very similar between those computed from surrogates trained from LHS or LPSS, with a maximum relative difference of 0.98% on the cross-flow load sensitivities or 0.002% on the base motion load sensitivities. This data (i.e., Workflows 2 and 3), along with the surrogate-based sensitivities established from FAST sampling (Workflow 1) is shown in Table 4 as well. Figure 13 and Figure 14 show the differences between the surrogate-based sensitivities and those from the full-order model. Aside from the lowest sample numbers (e.g., 27 or 64), increasing the sample size beyond 125 had an almost negligible effect on how well the surrogate-based sensitivities compared with the benchmark values computed directly from the full-order finite element analysis. This suggests that, for this stationary FIV problem, there is minimal accuracy to be gained of the sensitivity analysis results by u sing large sample sizes beyond those for which the surrogate model verification error cease to decrease beyond approximately 0.01 $\mu\epsilon$ (see Figure 7 compared to Figure 13 and Figure 14).

Next, Figure 15 and Figure 16 show the results associated with the surrogates trained from FAST sampling, LHS, and LPSS are overlaid on the same graph. Of significance is that even though the surrogates used to calculate these sensitivities were constructed from different sampling strategies, the resultant global sensitivities do not appreciably differ from one another which serves to demonstrate the stability of the GSA results.

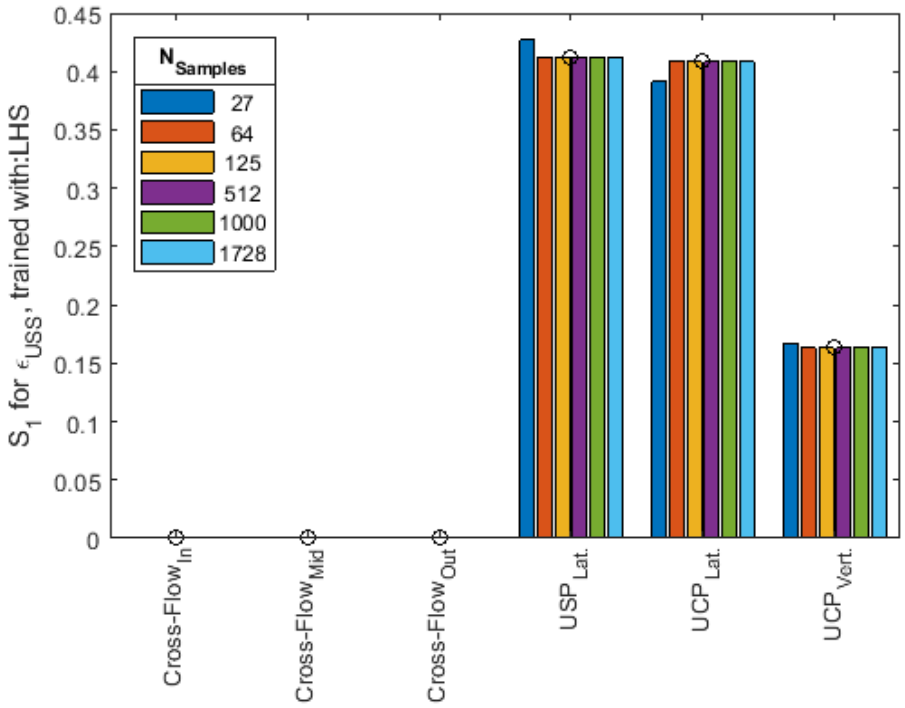

FIGURE 11 - COMPARISON OF SENSITIVITIES FROM LHS-TRAINED SURROGATE MODELS

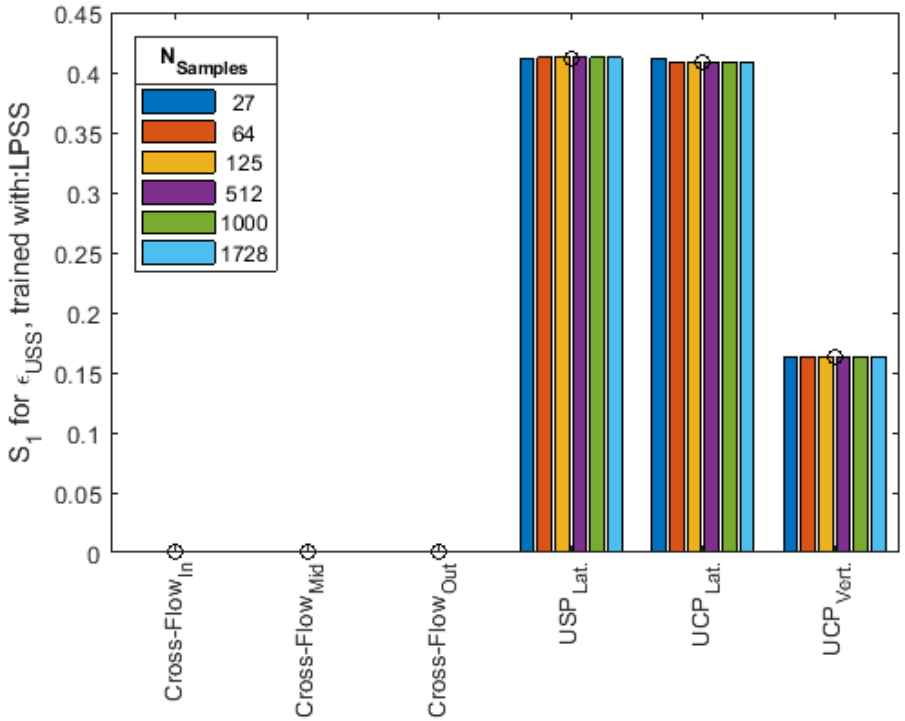

FIGURE 12 - COMPARISON OF SENSITIVITIES FROM LPSS-TRAINED SURROGATE MODELS

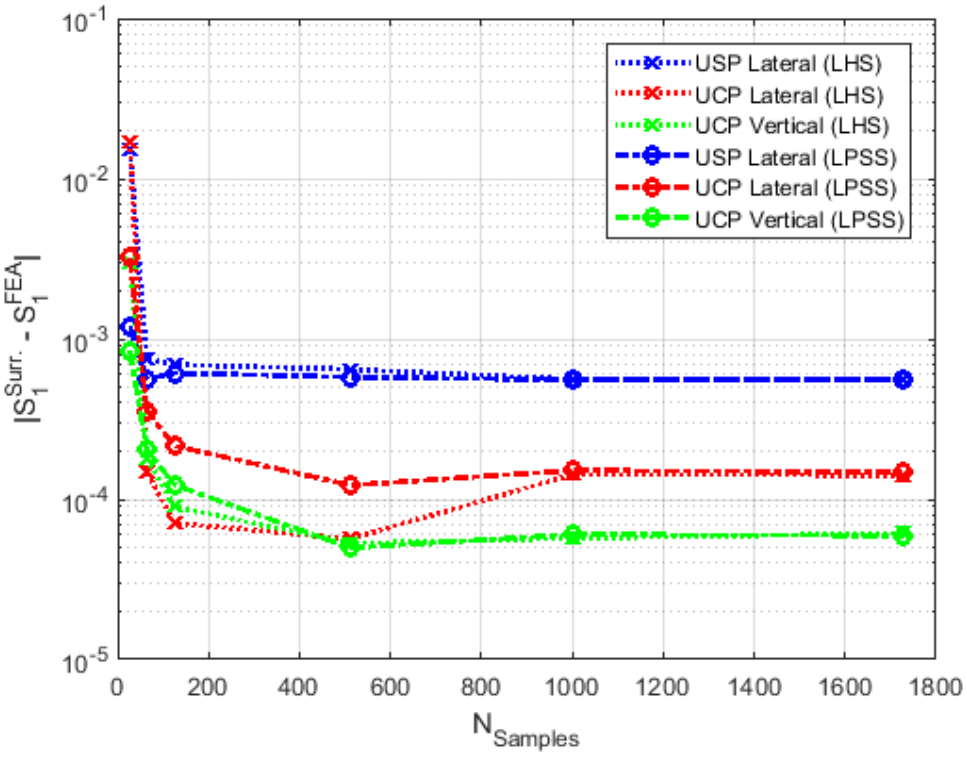

FIGURE 13 – COMPARISON OF LHS-TRAINED AND LPSS-TRAINED SURROGATE-BASED SENSITIVITIES TO BENCHMARK FOR BASE MOTION LOADS

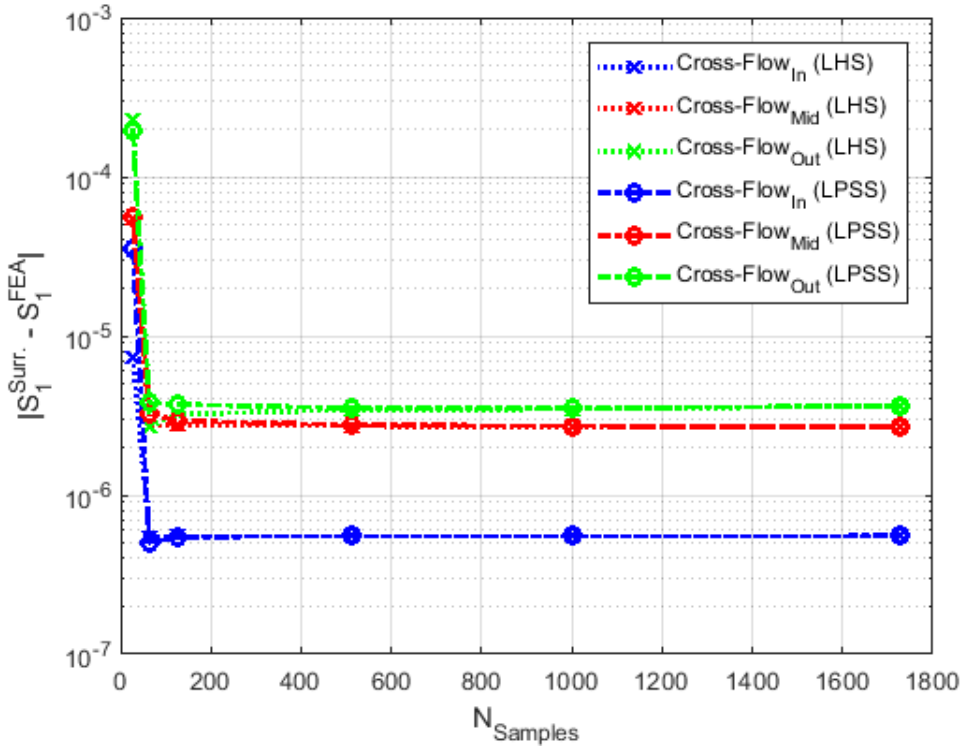

FIGURE 14 – COMPARISON OF LHS-TRAINED AND LPSS-TRAINED SURROGATE-BASED SENSITIVITIES TO BENCHMARK FOR CROSS-FLOW LOADS

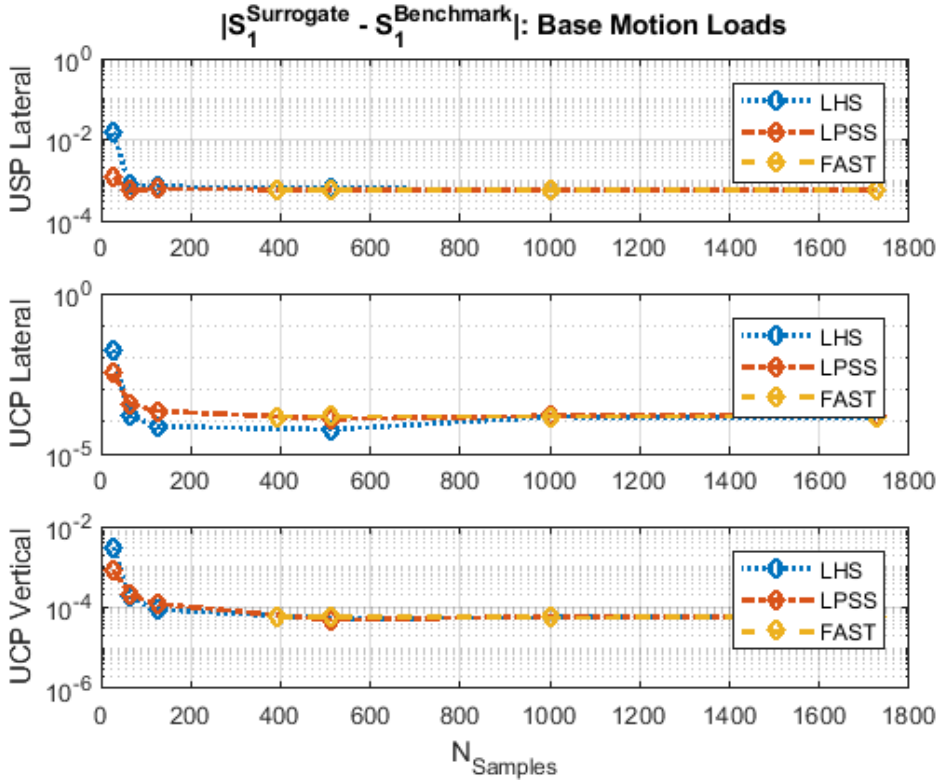

FIGURE 15 - SURROGATE-BASED SENSITIVITIES VS. BENCHMARK FOR BASE MOTION LOADS

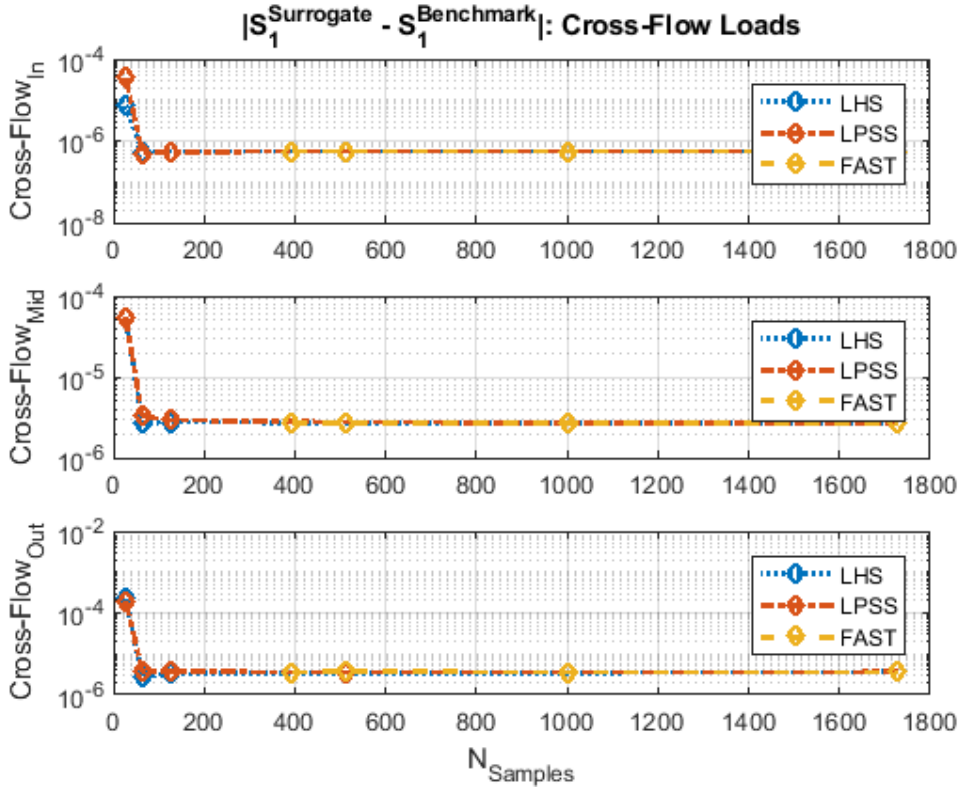

FIGURE 16 - SURROGATE-BASED SENSITIVITIES VS. BENCHMARK FOR CROSS-FLOW LOADS

TABLE 4
SENSITIVITY INDICES COMPUTED FROM SURROGATE MODELS

Forcing Function	$N_{FullOrderRuns}$	Cross-Flow (Inner)	Cross-Flow (Mid)	Cross-Flow (Outer)	Upper Support Plate Lateral	Upper Core Plate Lateral	Upper Core Plate Vertical	Sum
Kriging Model built from LPSS	27	3.61×10^{-5}	6.11×10^{-5}	2.53×10^{-4}	0.4107	0.4116	0.1626	0.985
	64	3.71×10^{-7}	2.58×10^{-6}	6.31×10^{-5}	0.4124	0.4087	0.1632	0.984
	125	3.24×10^{-7}	2.92×10^{-6}	6.30×10^{-5}	0.4125	0.4086	0.1633	0.984
	512	3.16×10^{-7}	3.09×10^{-6}	6.28×10^{-5}	0.4125	0.4085	0.1634	0.984
	1000	3.17×10^{-7}	3.13×10^{-6}	6.28×10^{-5}	0.4124	0.4085	0.1634	0.984
	1728	3.16×10^{-7}	3.15×10^{-6}	6.29×10^{-5}	0.4124	0.4085	0.1634	0.984
Kriging Model built from LHS	27	8.29×10^{-6}	6.04×10^{-5}	2.87×10^{-4}	0.4270	0.3912	0.1665	0.985
	64	3.21×10^{-7}	3.14×10^{-6}	6.19×10^{-5}	0.4126	0.4085	0.1633	0.984
	125	3.18×10^{-7}	3.08×10^{-6}	6.25×10^{-5}	0.4126	0.4084	0.1634	0.984
	512	3.16×10^{-7}	3.13×10^{-6}	6.27×10^{-5}	0.4125	0.4084	0.1634	0.984
	1000	3.17×10^{-7}	3.18×10^{-6}	6.27×10^{-5}	0.4124	0.4085	0.1634	0.984
	1728	3.18×10^{-7}	3.18×10^{-6}	6.29×10^{-5}	0.4124	0.4085	0.1634	0.984
Kriging Model built from FAST GSA samples	393	3.18×10^{-7}	3.20×10^{-6}	6.28×10^{-5}	0.4124	0.4085	0.1634	0.984
	512	3.16×10^{-7}	3.14×10^{-6}	6.30×10^{-5}	0.4124	0.4085	0.1634	0.984
	1000	3.17×10^{-7}	3.19×10^{-6}	6.28×10^{-5}	0.4124	0.4085	0.1634	0.984
	1728	3.17×10^{-7}	3.18×10^{-6}	6.29×10^{-5}	0.4124	0.4085	0.1634	0.984

Additional Discussion of Results

In addition to the physical insight offered by the GSA, the accuracy of the surrogate models which were constructed using designed computational experiments is compared with the convergence of the GSA results. Although at sample sizes of greater than 500, the differences in surrogate-based GSA results with respect to full-order model GSA results were shown to be small, and also insensitive to the method used to sample the parameter space (e.g., FAST, LHS, or LPSS), some noteworthy differences are observed for smaller sample sizes. From the results at smaller sample sizes, two items are noteworthy. First, LHS and LPSS reduce the number of samples needed to assess sensitivity as compared to sampling the parameter space directly with FAST. The minimum number of samples used for FAST was 393, based on the number of integration points needed to resolve the underlying periodic functions for the dimensionality of this problem. In terms of both the surrogate verification error and global sensitivities, LHS and LPSS provide comparable results at 64 samples. Second, for the very small sample size of 27 the error of the global sensitivities determined from the surrogate trained with LPSS is substantially lower than that trained with LHS. As such, although interaction effects may not be strong, the variance reduction provided by LPSS as compared with LHS for a very small number of samples is insightful.

The similar behavior amongst those three methods of sampling the parameter space, as well as the agreement between the surrogate-based sensitivities and those computed from the full-order model, provides confidence in the stability of the results. Furthermore, the agreement between sensitivity indices calculated by the surrogate and full-order models lends credence as to the veracity of the surrogate models. Although the surrogate verification error was quantified in terms of a strain value and the global sensitivity values are unitless, a comparison between these errors may be observed by comparing Figure 7 to Figure 10 for FAST, and to Figure 13 and Figure 14 for LHS and LPSS.

The downcomer forcing function has historically received significant interest (e.g., (Au-Yang & Jordan, 1980)), and to some extent this study helps to substantiate the significance of that particular forcing function. The downcomer forcing function acts directly upon lower internals components, such as the core barrel, and that motion is then coupled with upper internals components through the upper support flange. From this study, it is apparent that the downcomer forcing function not only directly affects the lower internals response (e.g., core barrel), but also manifests itself as a base motion load on the upper internals structures and proves even more dominant as a base motion load than the cross-flow loads acting directly upon the upper internals components. This is a meaningful observation in the sense that much effort has traditionally been devoted to characterizing flow fields in the upper plenum region of the reactor. It is thus apparent that from the perspective of the structural dynamic response of the upper support assembly subjected to flow-induced excitation, rigorous characterization of the upper plenum flow field may be, to some extent, unwarranted. As a caution, this point is not necessarily generalizable to all PWRs, but is nonetheless a meaningful observation for the particular analysis presented herein.

These observations have implications in terms of both nuclear component design and diagnostics. For design of a complex reactor assembly, characterization of forcing functions incurs significant engineering cost involving scale model test programs and computationally expensive computational fluid dynamics (CFD) simulations. Thus, if the forced response of a complex assembly is governed by a select few forcing functions, albeit of uncertain magnitude, a surrogate model defined by those forcing functions may be exercised easily to make risk informed decisions to focus on development of specific forcing functions during the design process. For diagnostics, dynamic instrumentation of an operating reactor incurs great cost to plant owners. Thus, if a given component is experiencing anomalous behavior, which is observable from its structural dynamic behavior, and it is known which few forcing functions govern the associated forced response, the amount of

required dynamic instrumentation may be limited in order to diagnose potential problems. Furthermore, an inverse problem may be constructed and parameterized so as to seek optimal, or most-likely, values of the dominant forcing functions.

Conclusions

A surrogate model prototypic of an upper internals reactor subassembly was constructed. This model included 6 independent forcing functions (with variance) and one output forced response variable (axial strain). The global sensitivity analyses showed that for the response variable of interests, three of the total six forcing functions dominate the response of the structure.

Three different workflows were studied in which the Kriging surrogates were trained using different methods of sampling the parameter space; namely FAST, LHS, and LPSS. For large sample sizes, all approaches converged to produce accurate global sensitivities which provides confidence in the model results and suggests a stable sensitivity analysis result. For relatively small sample sizes, LHS and LPSS were shown to yield surrogates with improved accuracy relative to those yielded from FAST. For very small sample sizes, LPSS is shown to yield improved accuracy relative to LHS.

The optimal selection of Kriging trend and correlation functions depends on the application at-hand. Recently, novel model selection criterion and model averaging technique that employs the information-theoretic multimodel inference have been documented (Sundar & Shields, 2018). Similarly, aggregate surrogate modeling methods adaptively trained by a unique universal predictive distribution have recently been documented in (Salem, et al., 2017) and (Salem & Tomaso, 2018), and initially explored in (Banyay, et al., 2018). Additional future planned work may thus involve the application of those and similar methods to those used herein for a reactor assembly model with non-linearities (i.e., non-linear springs and dampers) and non-stationary loading (i.e., loss-of-coolant-accident acoustic or seismic loads), with varying ranges of parameter perturbations.

References

Abbiati, G., Schobi, R., Sudret, B. & Stojadinivoc, B., 2017. *Structural Reliability Analysis using Deterministic Hybrid Simulations and Adaptive Kriging Metamodeling.* Santiago, Chile, Earthquake Engineering Research Institute.

ANSYS, 2016. *Mechanical APDL Theory Reference.* 17.1 ed. Canonsburg(PA): SAS IP, Inc..

ASME, 2009. *Standard for Verification and Validation in Computational Fluid Dynamics and Heat Transfer.* New York(NY): ASME.

ASME, 2017. *Rules for Construction of Nuclear Facility Components.* New York(NY): ASME.

Au-Yang, M. K., 2001. *Flow-Induced Vibration of Power and Process Plant Components.* New York(NY): ASME.

Au-Yang, M. K. & Connelly, W. H., 1977. A Computerized Method for Flow-Induced Random Vibration Analysis of Nuclear Reactor Internals. *Nuclear Engineering and Design,* Volume 42.

Au-Yang, M. K. & Jordan, K. B., 1980. Dynamic Pressure Inside a PWR – A Study Based on Laboratory and Field Test Data. *Nuclear Engineering and Design,* Volume 58, pp. 113-125.

Banyay, G. A., Meyer, G. A. & Walker, A. P., 2015. *Proposed Changes to the ASME Boiler and Pressure Vessel Code Section III Appendix N for Flow-Induced Vibrations.* Boston, MA, ASME.

Banyay, G. A., Smith, S. D. & Young, J. S., 2018. *Sensitivity Analysis of a Nuclear Reactor System Finite Element Model.* Minneapolis, MN, ASME.

Bendat, J. S. & Piersol, A. G., 2010. *Random Data: Analysis and Measurement Procedures.* 4 ed. Hoboken(NJ): John Wiley & Sons.

Blevins, R. D., 2001. *Flow-Induced Vibration.* 2 ed. Malabar(FL): Kreiger.

Cannavo, F., 2012. Sensitivity analysis for volcanic source modeling quality assessment and model selection. *Computers & Geosciences,* Volume 44, pp. 52-59.

Cheng, K. et al., 2017. Global sensitivity analysis using support vector regression. *Applied Mathematical Modeling,* September.Volume 49.

Cukier, R. I., Levine, H. B. & Shuler, K. E., 1978. Nonlinear Sensitivity Analysis of Multiparameter Model Systems. *Journal of Computational Physics,* Volume 16, pp. 1-42.

Gratiet, L. L., Marelli, S. & Sudret, B., 2016. *Metamodel-based Sensitivity Analysis: Polynomial Chaos Expansions and Gaussian Processes.* s.l.:ETH-Zurich.

Grigoriu, M., 2010. Linear random vibration by stochastic reduced-order models. *International Journal for Numerical Methods in Engineering,* Volume 82.

Grigoriu, M. & Field, R. V., 2014. A method for analysis of linear dynamic systems driven by stationary non-Gaussian noise with applications to turbulence-induced random vibration. *Applied Mathematical Modeling,* Volume 38.

Hou, Z., Lu, W. & Chen, M., 2016. Surrogate-Based Sensitivity Analysis and Uncertainty Analysis for DNAPL-Contaminated Aquifer Remediation. *Journal of Water Resources Planning and Management,* November.142(11).

Huang, Z., Wang, C., Chen, J. & Tian, H., 2011. Optimal design of aeroengine turbine disc basd on kriging surrogate models. *Computers & Structures,* Volume 89.

International Atomic Energy Agency, 2008. *Best Estimate Safety Analysis for Nuclear Power Plants: Uncertainty Evaluation.* [Online]
Available at: https://www-pub.iaea.org/MTCD/publications/PDF/Pub1306_web.pdf
[Accessed July 2018].

Lataniotis, C., Marelli, S. & Sudret, B., 2017. *UQLab User Manual – Kriging (Gaussian Process Modelling).* Zurich: ETH-Zurich.

Marelli, S. & Sudret, B., 2014. *UQLab: A framework for uncertainty quantification in Matlab.* Liverpool, UK, ASCE.

McRae, G. J., Tilden, J. W. & Seinfeld, J. H., 1980. Global Sensitivity Analysis – A Computational Implementation of the Fourier Amplitude Sensitivity Test (FAST). *Computers & Chemical Engineering.*

Montgomery, D. C., 2013. *Design and Analysis of Experiments.* 8 ed. Hoboken(NJ): John Wiley & Sons.

Morgan, M. G., Henrion, M. & Small, M., 1992. *Uncertainty: A Guide to Dealing with Uncertainty in Quantitative Risk and Policy Analysis.* Cambridge: Cambridge University Press.

Mulcahy, T. M., 1982. *Design Guide for Single Circular Cylinder in Turbulent Crossflow,* Lemont, IL: Argonne National Laboratory.

Nechak, L., Gillot, F., Besset, S. & Sinou, J. J., 2015. Sensitivity analysis and Kriging based models for robust stability analysis of brake systems. *Mechanics Research Communications,* Volume 69.

Ortiz, K., Wirsching, P. H. & Paez, T. L., 1995. *Random Vibrations: Theory and Practice.* New York(NY): John Wiley & Sons.

Paez, T. L., Tucker, S. & O'Gorman, C., 1997. *Simulation of Nonlinear Random Vibrations using Artificial Neural Networks,* Albuquerque, NM: Sandia National Laboratory.

Palamara, M. J. et al., 2015. *Development of an Advanced PWR Reactor Internals System Finite Element Model for Flow-Induced Vibration Analyses.* Boston, MA, ASME.

Pianosi, F., Sarrazin, F. & Wagener, T., 2015. A Matlab toolbox for Global Sensitivity Analysis. *Environmental Modeling & Software,* Volume 70.

Rajakumar, C. & Rogers, C. R., 1991. The Lanczos Algorithm Applied to Unsymmetric Generalized Eigenvalue Problems. *International Journal for Numercial Methods in Engineering,* Volume 32, pp. 1009-1026.

Rasmussen, C. E. & Williams, C. K., 2005. *Gaussian Processes for Machine Learning.* Cambridge(MA): MIT Press.

Sacks, J., Welch, W. J., Mitchell, T. J. & Wynn, H. P., 1989. Design and Analysis of Computer Experiments. *Statistical Science,* Volume 4, pp. 409-435.

Salem, M. B., Roustant, O., Gamboa, F. & Tomaso, L., 2017. Universal Prediction Distribution for Surrogate Models. *SIAM/ASA Journal on Uncertainty Quantification,* 5(1), pp. 1086-1109.

Salem, M. B. & Tomaso, L., 2018. Automatic selection for general surrogate models. *Structural and Multidisciplinary Optimization.*

Saltelli, A. et al., 2008. *Global Sensitivity Analysis: The Primer.* West Sussex, UK: John Wiley and Sons.

Schenk, C. A. & Schueller, G. I., 2005. *Uncertainty Assessment of Large Finite Element Systems.* Berlin: Springer-Verlag.

Shahsavani, D. & Grimvall, A., 2011. Variance-based sensitivity analysis of model outputs using surrogate models. *Environmental Modelling & Software,* June.26(6).

Shields, M. D. & Zhang, J., 2016. The Generalization of Latin Hypercube Sampling. *Reliability Engineering & System Safety,* Volume 148, pp. 96-108.

Sundar, V. S. & Shields, M. D., 2018. Reliability analysis using adaptive kriging surrogates with multimodel inference. *ASCE-ASME Journal of Risk and Uncertainty in Engineering Systems: Part A Civil Engineering.*

Tennekes, H. & Lumley, J. L., 1972. *A First Course in Turbulence.* Cambridge(MA): MIT Press.

United States Nuclear Regulatory Commission, 2013. *Programs for Monitoring Boiling-Water Reactor Steam Dryer Integrity*. [Online]
Available at: https://www.nrc.gov/docs/ML1300/ML13003A049.pdf
[Accessed July 2018].

United States Nuclear Regulatory Commission, 2015. *Review of Lessons Learned from the San Onofre Steam Generator Tube Degradation Event.* [Online]
Available at: https://www.nrc.gov/docs/ML1501/ML15015A419.pdf
[Accessed July 2018].

United States Nuclear Regulatory Commission, 2017. *Comprehensive Vibration Assessment Program for Reactor Internals during Preoperational and Initial Startup Testing.* Rockville(MD): United States Nuclear Regulatory Commission.

Westinghouse Electric Company, 2011. *AP1000 Design Control Document.* Cranberry Township(PA): Westinghouse Electric Company, LLC.

Westinghouse Electric Company, 2015. *Comprehensive Vibration Assessment Program (CVAP) Vibration Analysis Program for the AP1000 Plant.* Cranberry Township(PA): Westinghouse Electric Company, LLC.